ChemSusChem

Low temperature continuous flow dehydration of xylose over water-tolerant niobia-titania heterogeneous catalysts

--Manuscript Draft--

Manuscript Number:	
Article Type:	Full Paper
Corresponding Author:	Pierluigi Barbaro Consiglio Nazionale delle Ricerche Sesto Fiorentino, ITALY
Corresponding Author E-Mail:	pierluigi.barbaro@iccom.cnr.it
Order of Authors (with Contributor Roles):	Carmen Moreno-Marrodan
	Pierluigi Barbaro
	Stefano Caporali
	Filippo Bossola
Keywords:	sustainable chemistry; heterogeneous catalysis; biorenewable resources; continuous flow; xylose
Manuscript Classifications:	Heterogeneous catalysis; Renewable resources; Sustainable Chemistry
Suggested Reviewers:	Kazuki Nakanishi, Prof. Kyoto University kazuki@kuchem.kyoto-u.ac.jp Expert in unconventional hierarchically porous monolithic materials
	Paolo Fornasiero, Prof. University of Trieste pfornasiero@units.it Expert in heterogeneous catalysis
	Manuel Moliner Manuel Moliner, Dr. Consejo Superior de Investigaciones Científicas mmoliner@itq.upv.es Expert in catalysis by solid acids
	Pieter C. A. Bruijnincx, Prof. University of Utrecht p.c.a.bruijnincx@uu.nl Expert in catalytic conversion of biomass
	Johannes G. de Vries, Prof. Universität Rostock johannes.devries@catalysis.de Expert in sustainable conversion of renewables
Opposed Reviewers:	
Abstract:	The sustainable conversion of vegetable biomass-derived feeds to useful chemicals requires innovative routes matching environmental and economical criteria. The approach herein pursued is the synthesis of water-tolerant, unconventional solid acid monolithic catalysts based on a mixed niobia-titania skeleton building up a hierarchical open-cell network of meso and macropores, and tailored for use under continuous flow conditions. The materials were characterized by spectroscopic, microscopy and diffraction techniques showing a reproducible, isotropic structure and an increasing Lewis / Brønsted acid sites ratio with increasing Nb content. The catalytic dehydration reaction of xylose to furfural was investigated as representative application. The efficiency of the catalyst showed to be dramatically affected by the niobia content in the titania lattice. The presence of as low as 2% wt niobium resulted in ther highest furfural yield at 140 °C reaction temperature under continuous flow conditions, using H2O / Y-valerolactone as safe monophasic solvent system. The interception of a transient 2,5-anhydroxylose species suggested the dehydration process to occur via a cyclic

	intermediates mechanism. The catalytic activity and the formation of the anhydro intermediate were related to the LAS/BAS ratio and indicated a significant contribution of xylose-xylulose isomerization. No significant catalyst deactivation was observed over 4 days usage.
Author Comments:	Title:Low temperature continuous flow dehydration of xylose over water-tolerant niobia-titania heterogeneous catalysts Authors: Carmen Moreno-Marrodan, Pierluigi Barbaro, Stefano Caporali and Filippo Bossola Firenze June 25th, 2018 Dear Editor, the present manuscript describes the synthesis of new heterogeneous catalysts based on an unconventional mixed niobia-titania monolithic structure building up an open-cell network of meso and macropores, tailored for use under continuous flow conditions. The catalysts were thoroughly characterized by a combination of spectroscopic, microscopy and diffraction techniques. The materials were specifically selected for their solid acid properties and tolerance to water, hence for use in the catalytic conversion of biomass derivatives in the aqueous phase. The catalysts' performance was demonstrated in a challenging reaction of great current interest: the dehydration of xylose to furfural. The catalytic efficiency showed to be dramatically affected by the niobia content in the titania lattice, wherein optimal yields were observed for as low as 2% wt niobium, using H2O / Y-valerolactone as green monophasic solvent system. No significant catalyst deactivation was observed over four days usage. The heterogeneous catalyst herein described enables the title reaction to be carried out under continuous flow conditions, with performances that compare favourably with those reported in the literature, whereas it is usually carried out in batch using biphasic / toxic solvents (toluene, DMF, butanol), higher temperatures, or in the homogenous phase using sulphuric acid, thus representing a considerable benefit in terms of sustainability. Moreover, we have disclosed novel mechanistic insights of the xylose dehydration reaction. The 2,5-anhydroxylose intermediate was for the first time reported, indicating that the dehydration process occurs via a cyclic intermediates mechanism. The catalytic activity and the formation of the intermediate were rationalized in terms of high Lewis / Brønsted acid sites ratio and indicated a significant contribution of xylose-xylulose isomerisation. We believe that the present work may represent a significant contribution toward the development of new sustainable processes for the conversion of biomass feeds to platform chemicals and fuels, at the interface between material chemistry, heterogeneous catalysis, biorefinery applications and use of renewable sources, while providing useful advances in the design of innovative catalytic systems and in the understanding of their working. Therefore, we would be delighted if you may consider the present manuscript for publication in ChemSusChem as Full paper. The authors have no conflict of interest to declare. Many thanks for your work and attention, kindest regards Pierluigi Barbaro
Section/Category:	
Additional Information:	
Question	**Response**

Submitted solely to this journal?	Yes
Has there been a previous version?	No
Do you or any of your co-authors have a conflict of interest to declare?	No. The authors declare no conflict of interest.

Low temperature continuous flow dehydration of xylose over water-tolerant niobia-titania heterogeneous catalysts

Carmen Moreno-Marrodan,[a] Pierluigi Barbaro,*[a] Stefano Caporali,[b] and Filippo Bossola[c]

The sustainable conversion of vegetable biomass-derived feeds to useful chemicals requires innovative routes matching environmental and economical criteria. The approach herein pursued is the synthesis of water-tolerant, unconventional solid acid monolithic catalysts based on a mixed niobia-titania skeleton building up a hierarchical open-cell network of meso and macropores, and tailored for use under continuous flow conditions. The materials were characterized by spectroscopic, microscopy and diffraction techniques showing a reproducible, isotropic structure and an increasing Lewis / Brønsted acid sites ratio with increasing Nb content. The catalytic dehydration reaction of xylose to furfural was investigated as representative application. The efficiency of the catalyst showed to be dramatically affected by the niobia content in the titania lattice. The presence of as low as 2% wt niobium resulted in ther highest furfural yield at 140 °C reaction temperature under continuous flow conditions, using H_2O / γ-valerolactone as safe monophasic solvent system. The interception of a transient 2,5-anhydroxylose species suggested the dehydration process to occur via a cyclic intermediates mechanism. The catalytic activity and the formation of the anhydro intermediate were related to the LAS/BAS ratio and indicated a significant contribution of xylose-xylulose isomerization. No significant catalyst deactivation was observed over 4 days usage.

Introduction

A monolith is “a shaped, fabricated intractable article with a homogeneous microstructure that does not exhibit any structural components distinguishable by optical microscopy”.[1] According to this definition, conventional foams or honeycomb-type materials with millimetre size cavities,[2] commonly reported in the chemical engineering literature for gas-phase unselective thermal processes,[3,4] do not belong to this category. By contrast, unconventional monoliths with sub-millimetre scale porosity have been described in various flow-through applications for the fine chemistry, including chromatography and catalysis, thanks to the enhanced contact with molecular substrates because of the large surface area.[5] Particularly, monoliths featuring an isotropic, hierarchically porous network of narrowly size distributed, open-cell macropores (1-20 μm) and mesopores (2-50 nm) within the struts (1-5 μm)[6,7] feature a peculiar hydrodynamic behaviour joining the advantages of efficient processing, typical of mesoporous materials, and fast diffusion, due to macropores.[8,9] Compared to mesoporous-only materials, these monoliths provide considerable benefits in heterogeneous catalysis in terms of reduced pore clogging, better active sites accessibility and improved mass transfer.[10,11] When exposed to a continuous flow of a liquid phase, the pressure drop per unit reactor length ($\Delta P/L$) generated by a hierarchically porous monolith is ca. one order magnitude lower compared to the corresponding mesoporous material under the same flow conditions.[12] Based on the Darcy's law, this is attributed to the high permeability coefficient of hierarchically porous monoliths (k > 0.25 μm^2),[9] which is proportional to the macropore size ($\Delta P/L = \mu v/k$, μ viscosity; v linear velocity).[13]

The development of efficient, continuous flow reactor systems is critical in catalysis, due to the several advantages compared to batch operations including increased safety and reactor volume productivity, better heat transfer, reduced development time, improved process control, simpler downstream processing and smaller hold-up volumes (solvents, reagents).[14,15] Continuous refresh of catalyst surface may also significantly reduce active site inhibition due to adsorbed co-products.[16] Monolithic catalysts have shown to be particularly useful to this regard, as they overcome most issues typical of packed-bed systems, such as high backpressure evolution, low contacting efficiency, broad distribution of residence times, formation of hot-spots or stagnation zones, which result in uncontrolled fluid dynamics, hence in unsatisfactory performance.[17]

Polymeric materials were the first to prove the benefits of monoliths in catalysis.[18,19] However, they show several drawbacks, including limited thermal, mechanical and chemical stability, shrinking phenomena, porosity changes with swelling, which may result in non-uniform radial permeability and in significant pressure drop at high flow rates.[20,21] In order to circumvent these issues, different types of inorganic monoliths have been synthesized by spinodal decomposition showing improved resistance and rigidity.[22,23] Examples include silica,[24,25,26,27]

[a] Dr. C. Moreno-Marrodan, Dr. P. Barbaro
Consiglio Nazionale delle Ricerche, Istituto di Chimica dei Composti Organo Metallici,
Via Madonna del Piano 10, 50019 Sesto Fiorentino, Firenze (Italy)
E-mail: pierluigi.barbaro@iccom.cnr.it
[b] Dr. S. Caporali
Consorzio Interuniversitario Nazionale per la Scienza e Tecnologia dei Materiali, Via Giusti 9, 50121, Firenze
and Consiglio Nazionale delle Ricerche, Istituto dei Sistemi Complessi,
Via Madonna del Piano 10, 50019 Sesto Fiorentino, Firenze, Italy.
[c] Dr. F. Bossola
Consiglio Nazionale delle Ricerche, Istituto di Scienze e Tecnologie Molecolari, Via Golgi 19, 20133 Milano (Italy)
Supporting information for this article can be found under: http://dx.doi.org/10.1002/cctc.xxxx

alumina,[28,29,30] titania,[31,32] zirconium phosphate[33] and $AlPO_4$.[34] Despite of their advantages, use of hierarchically porous inorganic monoliths in flow catalysis has been scarcely investigated so far, being essentially explored for HPLC applications.[35,36] One reason for this is the hardly reproducible preparation of monoliths with 2 - 15 mm diameter to perform microsynthesis,[37,38] owing to the extreme structure sensitivity from the phase system composition.[39] Specific functionalization of the monolithic material may also be required for catalytic applications.[40]

Few functionalized inorganic monoliths with hierarchical porosity have been described, either bearing supported metal nanoparticles (Ag,[41] Pd[42,43]), for metal-type catalysis (e.g. hydrogenations), or grafted acidic/basic groups (-SO_3H, -NH_2, Al_2O_3, HPO_4^{2-}), for organic-type catalysis (e.g. dehydrations, condensations).[44,45] The catalytic performance of these monoliths has been compared with both packed-bed systems under continuous flow and with batch setups. The better productivity was clearly demonstrated for the monolithic systems in the Pd-catalyzed hydrogenation reaction of cyclohexene,[46,47] for metal-free trans-esterification, Knoevenagel,[48,49] Diels-Alder[50] and Friedländer reactions.[51] In terms of selectivity, Pd@SiO_2 monolith also performed better than Pd onto conventional mesoporous silica in the partial hydrogenation reaction of 3-hexyn-1-ol and 3-halogeno-nitrobenzenes, both under flow and batch conditions.[52] Irrespective of the supported catalyst and reaction, monolithic systems have shown remarkable stability for prolonged reaction times, with no significant activity decay observed up to 3 days time-on-stream.[46,50] All the above findings show the advantages of unconventional inorganic monolithic catalysts compared to the classical heterogeneous ones.[53]

Solid acid catalysis is of paramount importance in both the hydrocarbon[54,55] and the biorefinery industry, wherein conversion of real feedstocks (e.g. aqueous solution of carbohydrates),[56,57] usually requires tolerance to water and to medium-high temperatures.[58] Prompted by the low efficiency and the unsatisfactory thermal stability of the previously reported monolithic acid catalysts (i.e. zirconium phosphate[45] and sulfonated silica[59]), we sought to develop alternative materials with improved performance for the conversion of biomass-derived substrates under continuous flow conditions. Herein, we report the first example of 3D isotropic, niobia-titania monoliths featuring a well-defined, hierarchically porous structure with interconnected meso and macropores. Choice of mixed titanium-niobium oxide materials has multiple motivations: the reproducible synthesis of titania monoliths (see above), the thermal and chemical stability of TiO_2,[60,61] the strong solid acid properties,[62,63] tolerance to water[64] and catalytic activity of Nb_2O_5,[65,66] the fast deactivation of pure niobia catalysts.[67] Other potentially useful properties for further catalytic applications include the strong metal-support interaction (SMSI) of both TiO_2[68] and Nb_2O_5,[69] the strong metal-promoter interaction (SMPI) of niobia,[70,71] the photocatalytic activity of titanium and niobium oxides.[72,73]

Mixed niobia-titania materials have some precedents in the literature with a Nb loading up to 40% atomic percentage. These include thin films, ceramic pellets, mesoporous and hierarchically micro(meso)macroporous powders. Most materials are based on niobium oxide layered onto preformed TiO_2 supports,[74,75,76] although few mixed oxides have also been reported.[77,78,79,80] Applications focused on sensing[81,82] and photocatalysis.[83] Studies in chemocatalysis were restricted to unselective oxidative processes under batch (e.g. propane dehydrogenation)[84] and in gas-phase continuous flow conditions (butan-1-ol[85,86] and toluene total oxidation[87]).

In the present work, the mixed niobia-titania monoliths synthesized were carefully characterized and their catalytic activity was demonstrated under continuous flow in the liquid phase, using a reaction of great relevance to the development of sustainable methods for biomass valorisation, i.e. the acid-catalyzed dehydration reaction of xylose to furfural, as representative example.

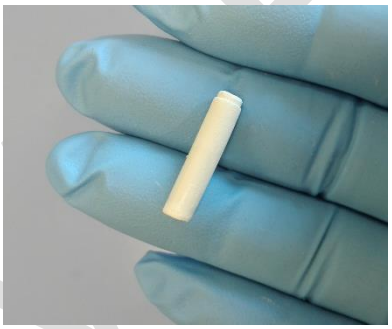

Figure 1. Optical image of dual porosity niobium-titanium oxide monolith.

Table 1. Mesoporosity features of monolithic materials.[a]

Monolith	D [nm]	V [$cm^3\ g^{-1}$]	S [$m^2\ g^{-1}$]
TiO_2-MNL	3.8 ± 0.2	0.20 ± 0.02	154 ± 9
NbTiO-MNL1	3.9 ± 0.6	0.20 ± 0.03	146 ± 5
NbTiO-MNL2	4.0 ± 0.4	0.20 ± 0.01	145 ± 4

[a] Pore diameter (D), porous volume (V), BET surface area (S).

Results and discussion

Synthesis and characterization of the hierarchically porous niobium-titanium oxide monoliths

Bimodal macro-mesoporous, mixed oxides monoliths (NbTiO-MNL, typically 5 mm diameter, 30 mm length, ca. 480 mg, Figure 1) were synthesized by a combination of spinodal decomposition and sol-gel transition method.[88] Thus, polymerization-induced phase separation and gelation of a composition-modulated $NbCl_5$-TPO–NMFA–PEO water-phase system led to the reproducible formation of monoliths of desired size. A labelling scheme was adopted according to the niobium molar content % of the starting reaction mixture (Table 1). As previously reported for other inorganic oxides, the procedure allowed to reinforce the monolith skeleton, resulting in the formation of uniform and crack-free materials featuring a hierarchically

porous structure.[39,46] During thermal treatment in the aging stage, temperature was cautiously kept below 350 °C, since the high acid strength of hydrated niobium pentoxide (Hammett acidity $H_0 \approx$ - 5.6, comparable to that of 70% H_2SO_4) is known to be drastically reduced above 500 °C.[89,90]

The as-prepared monoliths were thoroughly characterized by a combination of spectroscopic, microscopy and analytical techniques.

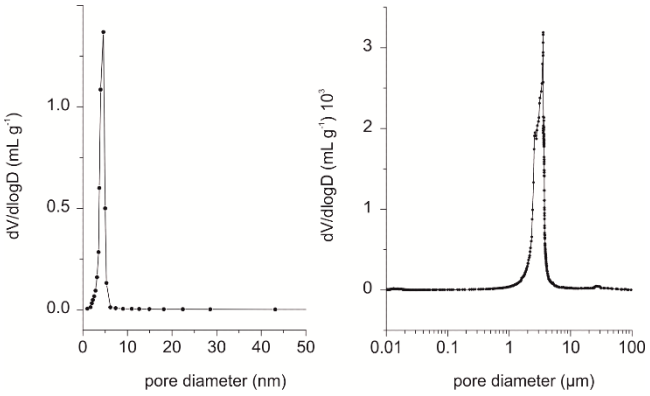

Figure 2. Pore size distribution in NbTiO-MNL2: mesopores size calculated from the N_2 desorption branch using the BJH method (left) and macropores size from mercury porosimetry (right).

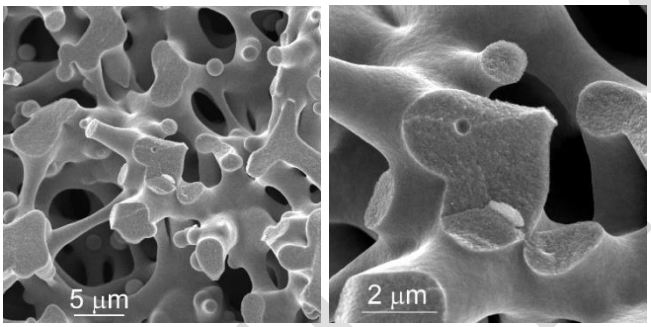

Figure 3. Typical SEM images of NbTiO-MNL2 (secondary electrons, 5 keV, high vacuum). Left: 11000 magnifications. Right: 29000 magnifications.

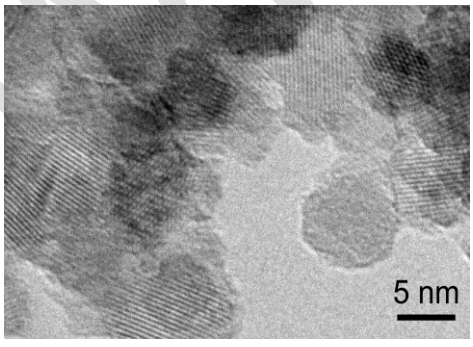

Figure 4. Typical TEM image of NbTiO-MNL2 (200 keV).

Textural properties. Porosity and morphology of the monoliths were investigated by N_2 porosimetry, mercury intrusion, X-ray microtomography, scanning and transmission electron microscopy.

Nitrogen isotherms showed the presence of narrow distributions of mesopores with average pore diameter 3-4 nm, connected through windows of ca. 2 nm, corresponding to 0.1-0.2 $cm^3\ g^{-1}$ cumulative pore volumes and 136-154 $m^2\ g^{-1}$ BET surface areas. Selected porosity data are reported in Table 1. The mesopores size distribution of NbTiO-MNL2 is reported in Figure 2 left, as representative example. No significant changes of mesopore width, volume or surface area were detected up to 2% niobium content.

SEM analysis showed the monoliths to have a well-defined, isotropic co-continuous microstructure consisting in a skeleton of ca. 3 μm thickness, forming an open-cell network of macropores of average size of ca. 4 μm.[91] Representative SEM images are reported in Figure 3 for NbTiO-MNL2. Neither aggregates of globular particles within the struts, nor significant morphologic differences were detected by SEM up to 2% Nb loading.[92]

The macroporosity and mechanical stability of the monoliths were examined by Hg intrusion measurements, showing narrow distributions of macropore diameters with mean values of 3 μm, in fair agreement with SEM evidences. The pore size diagram of NbTiO-MNL2 is reported in Figure 2, right, as example. In that case, the total macroporous volume and surface area were 0.56 $cm^3\ g^{-1}$ and 2.09 $m^2\ g^{-1}$, respectively, corresponding to an overall porosity of 53.7%.

TEM analysis showed the monoliths skeleton to be formed by spherical crystallites of 4-7 nm size building up the mesopores cavities. The nanocrystals are attached with no preferred orientation. A TEM image of NbTiO-MNL2 is reported in Figure 4. No significant difference of crystallite size was displayed by TEM analysis of monoliths with different Nb loadings.

The overall morphology of the monoliths was confirmed by X-ray tomography, which showed an isotropic, uniform radial distribution of voids and struts, and a very narrow size distribution of windows and diffusion pores. The data calculated were in line with those obtained from SEM and Hg porosimtery. In the case of NbTiO-MNL2 an average 5 μm skeleton thickness and 5 μm macropores diameter were obtained, corresponding to a total porosity of 49%.[46] A tomography reconstruction image of NbTiO-MNL2 is reported in Figure 5.

Figure 5. X-ray tomography 3D-reconstruction image of NbTiO-MNL2.

Table 2. Actual bulk composition of monolithic materials.[a]

Monolith	Nb [wt%]	Ti [wt%]	Ti / Nb molar ratio
TiO_2-MNL	-	59.8 ± 0.4	-
NbTiO-MNL1	1.0 ± 0.1	83.5 ± 0.4	162.1 ± 0.2
NbTiO-MNL2	2.0 ± 0.3	84.6 ± 0.4	82.1 ± 0.4

[a] Data from ICP-OES analysis. Mean values over three samples.

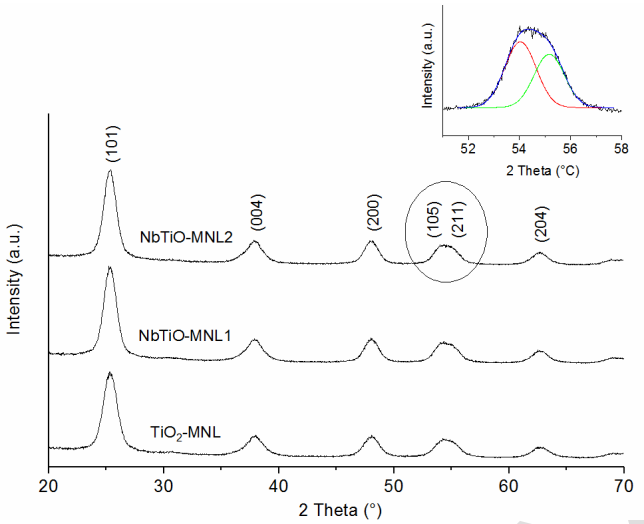

Figure 6. XRD patterns of niobia-titania monoliths. The inset is the deconvoluted peak in the (105) and (211) region for NbTiO-MNL2.

Table 3. Selected XRD properties of monolithic materials.

Monolith	2 Theta [°]		Crystallite size [nm]
	(105)	(211)	
TiO_2-MNL	54.28	55.42	6.8
NbTiO-MNL1	54.09	55.25	7.2
NbTiO-MNL2	54.03	55.16	7.4

Chemical composition. The composition of the monoliths was analyzed by ICP-OES, EDS, XRD and XPS.

Irrespective of the Nb loading, bulk ICP-OES analyses revealed the solids to have a metal content in line with that of the starting reaction mixture, thus indicating the quantitative incorporation of Nb and Ti into the monoliths. Representative data are reported in Table 2. The values of the Ti / Nb ratio (82-162) indicated the niobium content to be well below the reported solubility limit of Nb into anatase materials (ca. 4) in any case,[83,95] which is fair agreement with the absence of different phases detected in the XRD spectra (vide infra). EDS analyses, either multipoint or 2D maps, were in agreement with ICP-OES data within the experimental errors, showing homogeneous radial and longitudinal compositions within the monoliths. No elements other than Nb, Ti and O were detected above the sensitivity limit of the instrument (0.1% wt).

The XRD patterns of all monolithic materials showed the characteristic peaks of anatase-type crystalline TiO_2 due to (1 0 1), (0 0 4) and (2 0 0) reflections at 2θ of 25.39°, 38.01° and 48.00°, respectively (Figure 6). This indicates that the anatase phase is retained upon incorporation of up 2% wt Nb, as previously reported for similar niobium concentrations in other Nb-doped TiO_2 materials.[85,87] A weak peak at 2θ = 30.8° was detected, attributable to the (1 2 1) diffraction plane of brookite phase. The calculated percentage of brookite in the monoliths was less than 1 wt% in any case. No other phases, such as Nb_2O_5, were observed in the XRD profiles. The peak at ca. 55° could be deconvoluted into two components, corresponding to the (105) and (211) diffraction planes, which showed small shifts to lower 2θ values with increasing niobium content (Table 3). According to the Bragg's law, this can be explained in terms of replacement of Ti^{4+} (0.61 Å) by larger Nb^{5+} (0.64 Å) ions in the titania lattice.[81,93] The size of crystallites in the monolithic materials, calculated using the Debye-Scherrer formula, showed the crystallite size to slightly increase with niobium loading (Table 3), as previously reported.[94]

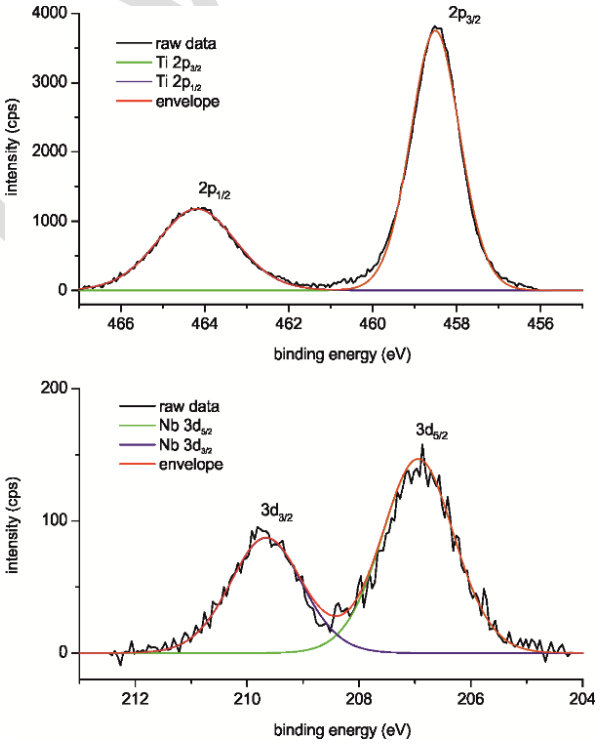

Figure 7. XPS spectrum and curve fit of NbTiO-MNL2 in the Ti 2p (top) and Nb 3d (bottom) regions.

Table 4. Selected XPS binding energy data [eV] for niobia-titania materials

Material	Nb		Ti		ref.
	$3d_{5/2}$	coupling	$2p_{3/2}$	coupling	
NbTiO-MNL1	206.9	2.7	458.5	5.7	this work
NbTiO-MNL2	206.9	2.7	458.4	5.7	this work
Nb_2O_5	207.3	2.8			[95]
TiO_2			459.3	6.2	[96]

Table 5. Lewis (LAS) and Brønsted (BAS) acid sites concentration on monolithic materials.[a]

Monolith	LAS [μmol g^{-1}]	BAS [μmol g^{-1}]	LAS / BAS ratio
TiO_2-MNL	244	22	11
NbTiO-MNL1	241	8	30
NbTiO-MNL2	160	1	160

[a] From FT-IR pyridine-desorption at 150 °C. LAS 1448 cm^{-1}, BAS 1540 cm^{-1}.

XPS measurements were carried out on all monolithic samples in order to define the oxidation state of the species involved. Representative XPS spectra and the curve fittings in the Ti 2p and Nb 3d regions, where the usual doublets are observed, are reported in Figure 7 for NbTiO-MNL2. Regardless of the niobium content, all spectra could be deconvoluted in one component only, whose binding energy values are in agreement with those previously reported for other Nb-doped TiO_2 anatase materials for Nb(V) (Nb $3d_{5/2}$ 206.9 ± 0.1 eV, spin-orbit coupling 2.7 eV) and Ti(IV) (Ti $2p_{3/2}$ 458.5 ± 0.1 eV spin-orbit coupling 5.7 eV).[77,85] Significant data are summarized in Table 4. No peaks attributable to other oxidation states, namely Nb(IV) and Ti(III), were detected above the detection limit of the technique. The observed binding energies were somewhat lower than those of pure Nb_2O_5[95] and anatase TiO_2[96] (Table 4), which can be attributed to a minor lowering of local symmetry due to the substitution of slightly larger Nb^{5+} ions for Ti^{4+} in the anatase network.[83] It was previously suggested that, when Nb^{5+} replace Ti^{4+} into a TiO_2 lattice, the excess of positive charge may be compensated either by the creation of one Ti cation vacancy for every four Nb^{5+} ions, by the reduction of one Ti atom from (IV) to (III) oxidation state for every Nb^{5+} ion, or by incorporation of one interstitial oxygen per two Nb^{5+} ions, with the formation of vacancies being the preferred mechanism for up to 10 at.% Nb content.[97,98] In all monolithic samples, the Ti / Nb molar ratios evaluated from XPS data was in fair agreement with those obtained from ICP-OES analysis within the experimental errors, which indicates a uniform surface / bulk composition.[99]

Acid capacity. The concentration of Lewis (LAS) and Brønsted (BAS) solid acid sites in the NbTiO monoliths was investigated by pyridine desorption FT-IR spectroscopy experiments at 150 °C.[100] Integration of peaks at 1540 and 1448 cm^{-1} revealed a moderate and a high concentration of Brønsted (22-1 μmol g^{-1}) and Lewis acid sites (244-160 μmol g^{-1}), respectively (Table 5).[101] The overall acid density showed to decrease with increasing Nb content, i.e. TiO_2-MNL > NbTiO-MNL1 > NbTiO-MNL2, while the LAS / BAS ratio (11-160) significantly increased in the same order.

Anatase TiO_2 has been reported to have weak acidic properties, significantly dependent from its structure and morphology, thus to be strongly affected by the preparation method.[102,103] The acidity of $Nb_2O_5 \cdot nH_2O$ has been examined in greater detail. The structure of niobium pentoxide is mainly composed of distorted NbO_6 octahedra and NbO_4 tetrahedra. While NbO_4 tetrahedra function as Lewis acid sites, the highly polarized Nb-O bonds in octahedra cause part of the surface OH groups to act as Brønsted acid sites.[104,105] The solid acid activity of both sites in water have been demonstrated in several instances.[104,106,107] The acidic properties of niobic acid depend on its thermal treatment. Brønsted and Lewis acid densities are highest at 100 °C and 300 °C, respectively, while decrease until being almost negligible at 500 °C,[90 which is in fair agreement with our results.

The ratio between the amount of Lewis and Brønsted sites have been previously quantified in other porous mixed niobium-titanium oxide materials, showing a trend analogous to that observed in the monoliths herein described, in the same Nb content range.[85 Although not exactly comparable with our materials, previous studies on titania-supported niobium oxide revealed the absence of BAS and a non linear decrease of LAS with niobia loading, that was explained in terms of partial replacement of existing sites.[108]

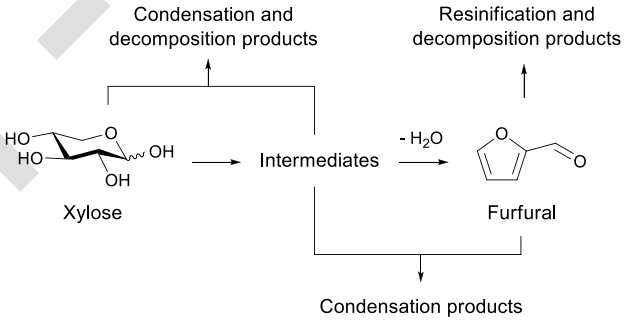

Scheme 1. Pathways for the acid-catalyzed dehydration reaction of xylose to furfural.

Catalytic dehydration of xylose to furfural

In order to evaluate the catalytic performance of the niobium-titanium oxide monoliths under continuous flow conditions, as well as the effect of niobia presence in the titania lattice, a representative reaction of great relevance to the valorisation of vegetable biomass was used,[109,110] namely the dehydration of xylose to furfural.

Furfural is an important platform chemical obtainable from hemicellulose-derived xylose via challenging threefold acid-catalyzed dehydration at high temperatures.[111,112] Current production methods rely on aqueous phase batch operations and use of homogeneous mineral acids (H_2SO_4).[113,114] Several oil-alternative, key industrial intermediates and consumer chemicals are accessible through further furfural processing.[115,116] Despite the significance of the reaction and the number of in-depth studies performed, the mechanism of xylose dehydration is not yet definitely agreed and several possibilities have been hypothesized.[117] A generally accepted pathway is sketched in Scheme 1.[118] It was

suggested that xylose undergoes a Brønsted acid-catalyzed conversion to various (anhydro) intermediates and other decomposition products,[119] followed by dehydration to furfural. It is known that the presence of Lewis acids increases the xylose-furfural conversion rate via isomerization to xylulose.[120,121] The selectivity of the process is limited by a number of side-reactions, including condensation of xylose and furfural with intermediates, decompositions, oligomerisations and resinifications.[122,123] The formation of unidentified by-products, such as solid humins or polymers, is responsible for the difference usually observed between the amount of xylose consumed and products detected in solution.

The Nb_2O_5-TiO_2 monoliths were scrutinized under a variety of flow conditions by modifying the reaction temperature, the residence time τ (i.e. the amount of time that the feed spends inside the reactor depending on the substrate solution flow rate),[124] and the combinations thereof. Thus, after cladding the monolith with a heat shrinkable Teflon tube and connecting to a continuous flow system, a stream of xylose solution in water : GVL = 1 : 9 (v/v) was allowed to flow through the monoliths under controlled conditions (Figure S6). Under our experimental conditions, highly reproducible flow patterns were observed within very short equilibration times. The reaction mixture collected at the outlet of the reactor was periodically analyzed via HPLC, GC-Ms and ICP-OES. Choice of the solvent mixture was motivated by the use of water as real xylose feed and by the fact that the addition of organic solvents is known to improve the selectivity of the acid-mediated xylose dehydration.[125,126] GVL (γ-valerolactone) is a water miscible, safe solvent obtainable from lignocellulosic biomass via catalytic methods.[127,128] Compared to pure water, benefits of water-GVL mixtures in terms of furfural selectivity have been attributed to the decrease in the activation energy of xylose dehydration and the increase of that of furfural degradation, on the basis of kinetic studies using both homogeneous and heterogeneous, Brønsted and Lewis catalysts.[129]

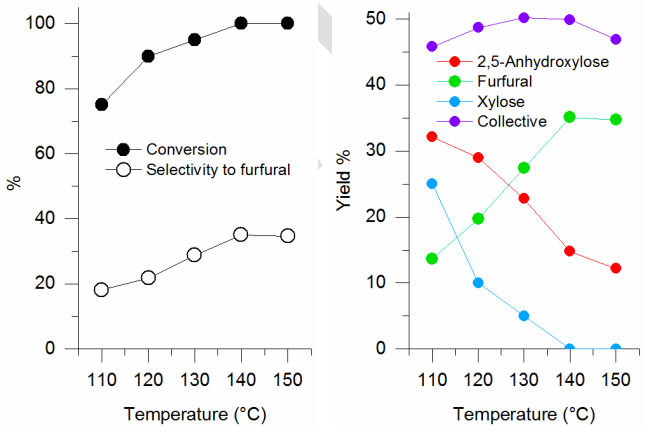

Figure 8. Selected data for the dehydration reaction of xylose over NbTiO-MNL2 catalyst under continuous flow conditions. Effect of temperature at fixed residence time (τ 85 s, xylose 0.02 M in H_2O : GVL = 1:9 v/v, average values over three experiments). Left: conversion and selectivity to furfural. Right: xylose, 2,5-anhydroxylose, furfural and collective yield of dehydration products.

Effect of the reaction temperature. The xylose dehydration reaction was investigated under fixed residence times in the temperature range 100 - 150 °C. The xylose conversion and the selectivity to furfural observed at τ 85 s are reported in graphical format in Figure 8, left, for NbTiO-MNL2 catalyst, as representative example, whereas the reaction solution composition is reported in Figure 8, right. Furfural selectivity was calculated as:

$$\text{Sel. (furfural)} = \frac{C_o\ \text{(furfural)}}{C_i\text{(xylose)} - C_o\ \text{(xylose)}} \cdot 100$$

where C_o and C_i are the observed and initial concentrations, respectively. In addition to xylose, the only compounds detected were furfural and the mono-dehydration product 2,5-anhydroxylose (GC-MS, Figure S7). The formation of insoluble humins was indicated by a brownish colouring of the solid catalyst.[130] In line with reported batch studies, the overall amount of dehydrated products (furfural and 2,5-anhydroxylose) corresponded to ca. a 50% yield, consistently with a significant contribution of side reactions.[131] Both conversion (up to 100%) and selectivity to furfural (up to 35%) increased with increasing reaction temperature, with a maximum observed at 140 °C. Selectivity slightly decreased above that temperature. If these data confirm that the xylose conversion process is favoured by high temperatures, two justifications can be found for the observed selectivity trend. On one hand, the concentration of furfural increased with increasing reaction temperature at the expenses of a decreasing concentration of 2,5-anhydroxylose (Figure 8, right). On the other hand, it is known that xylose dehydration is faster than furfural loss reactions (e.g. resinification) at high temperatures, which is called "entropy effect".[132,133] As a matter of fact, the collective yield of dehydration products (2,5-anhydroxylose plus furfural) reached a maximum at ca. 130 °C. Above 140 °C, the yield of furfural decreased, likely due to decomposition.[134] The detection of the 2,5-anhydroxylose intermediate indicates that the first dehydration step of xylose is faster than the further dehydrations (Scheme 2). Earlier kinetic studies of H_2SO_4-catalyzed xylose dehydration in water confirms this hypothesis.[135] Analogous findings have been reported for the two-fold dehydration reaction of sorbitol to isosorbide via 1,4-sorbitan.[136,137]

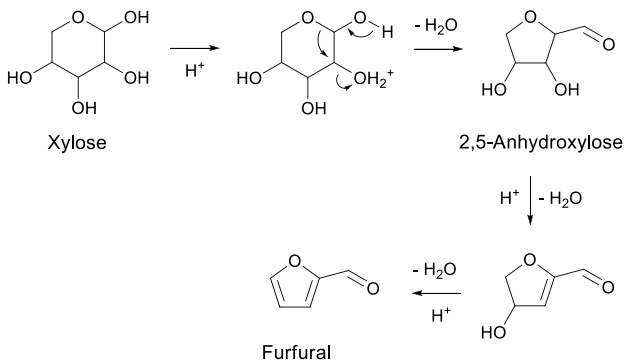

Scheme 2. Acid-catalyzed xylose dehydration mechanism via cyclic intermediates. Adapted from Ref [117] - Published by The Royal Society of Chemistry.

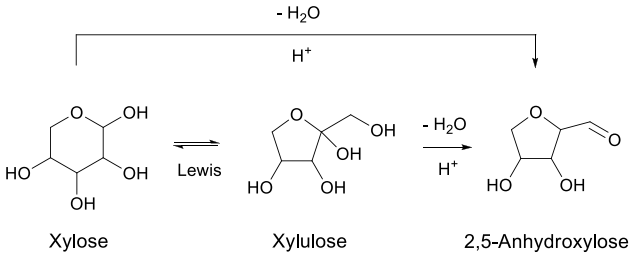

Scheme 3. Dehydration of xylose via isomerization to xylulose.

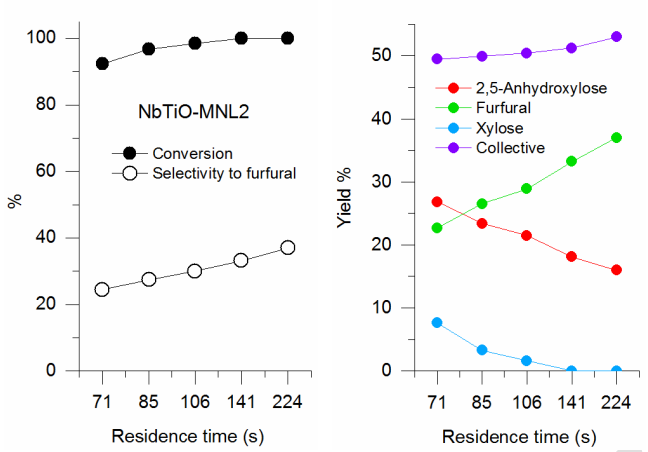

Figure 9. Selected data for the dehydration reaction of xylose over NbTiO-MNL2 catalyst under continuous flow conditions. Effect of residence time at fixed reaction temperature (130 °C, xylose 0.02 M in H_2O : GVL = 1:9 v/v, average values over three experiments). Left: conversion and selectivity to furfural. Right: xylose, 2,5-anhydroxylose, furfural and collective yield of dehydration products.

Interception of the 2,5-anhydroxylose supports that, at least under our experimental conditions, the dehydration of xylose occurs via a “cyclic intermediates rearrangement" mechanism (Scheme 2),[138,139] that was suggested to be energetically more favourable compared to a "dehydration of acyclic intermediates” one.[140,141] Nonetheless, we cannot rule out a contribution to the mechanism based on xylose-xylulose isomerisation followed by dehydration, due to the combined action of Lewis and Brønsted acid sites (Scheme 3).[142,143,144] Actually, minor amounts of xylulose (< 2%) were only detected using the monolithic catalyst with the highest LAS / BAS ratio, i.e. NbTiO-MNL2. To the best of our knowledge, the formation of the 2,5-anhydroxylose intermediate, despite being proposed in various studies,[115,116] has never been demonstrated by direct observation during acid-catalyzed xylose dehydration. 2,5-Anhydroxylose can be isolated by Swern oxidation of anhydroarabitol in two steps,[145] or in 15% yield from sugarcane bagasse after extraction with aqueous ethanol.[146] The fact that in our system the rate of formation of 2,5-anhydroxylose is higher than the rate of its further dehydration can be tentatively attributed to the unusually high LAS/BAS ratio (160), which enables fast 2,5-anhydroxylose formation via Lewis acid-catalyzed xylose-xylulose isomerisation (Scheme 3).

Effect of the residence time. The continuous flow dehydration reaction of xylose using monolithic catalysts was examined in the residence time range 71-224 s (0.4-0.1 mL min^{-1}), under fixed reaction temperature. No backpressure was generated by the monolithic reactors at these solution flow rates. Selected data at 130 °C for the NbTiO-MNL2 catalyst are shown in Figure 9, as representative example. The effect of residence time change was similar to that above described for the reaction temperature. An increase of the residence time, i.e. a longer contact time between catalyst and substrate, resulted in increasing xylose conversion and selectivity to furfural. Full conversion was achieved for τ 141 s. No selectivity decrease was observed up to τ 224 s (0.1 mL min^{-1}). At this residence time value, the furfural and the dehydration product collective yields were 37% and 53%, respectively. The yield of furfural increased with increasing residence time, at the expenses of the concentration of the transient 2,5-anhydroxylose specie.

Overall, the combination of reaction conditions resulting in the best, non-optimized (i.e. within the temperature and τ ranges examined) furfural yield of 39% was 140 °C and 224 s residence time.

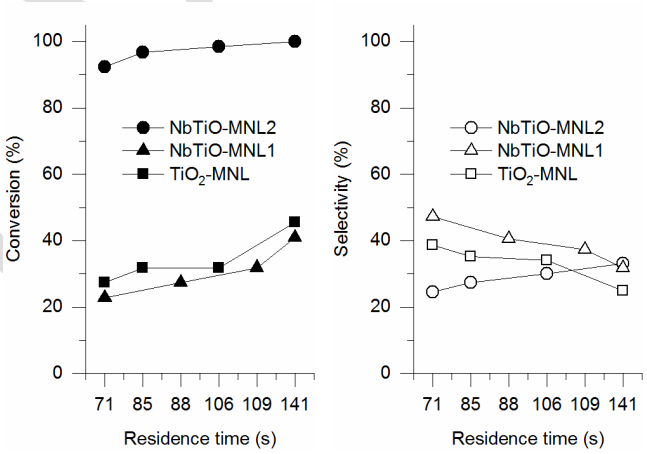

Figure 10. Selected data for the continuous flow dehydration reaction of xylose over monolithic catalysts at different residence times (130 °C, xylose 0.02 M in H_2O : GVL = 1:9 v/v, average values over three experiments). Left: conversion. Right: selectivity to furfural.

Comparison among monolithic catalysts. The monolithic materials showed significantly different performance in the catalytic dehydration reaction of furfural. Representative data are reported in graphical format in Figure 10. As above described for NbTiO-MNL2, xylose conversion increased with increasing residence time using both NbTiO-MNL1 and TiO_2-MNL, however with remarkably lower values in the same τ range (20-45%) (Figure 10, left). By contrast, while selectivities to furfural were in the same range observed using NbTiO-MNL2, their values decreased with increasing τ (Figure 10, right) using NbTiO-MNL1 and TiO_2-MNL, due to the formation of higher amounts of by-products (see Supporting Information). Compared to NbTiO-MNL2, selectivities at the same conversion level were therefore much lower using the NbTiO-MNL1 and TiO_2-MNL catalysts. A similar behaviour was observed

Table 6. Continuous flow dehydration reaction of xylose to furfural using monolithic catalysts under identical conditions.[a]

	Catalyst	Conversion [b] [%]	Dehydration yield [c] [%]	Furfural yield [%]	Selectivity [d] [%]	Productivity [e] [mol g^{-1} h^{-1}]·10^3	STY [f] [kg L^{-1} h^{-1}]·10^3
1	TiO_2-MNL [h]	31	22	11	34	0.1	7.2
2	NbTiO-MNL1 [i]	32	22	12	37	0.1	7.6
3	NbTiO-MNL2 [l]	98	50	29	30	0.2	19.0

[a] Reaction conditions: xylose 0.02 M in H_2O : GVL = 1:9 v/v, 0.1-0.4 mL min^{-1}, residence time τ = 106 s, 130 °C. Start time: attainment of steady state conditions ca. 0.5 h. Data from HPLC analysis. [b] Conversion average value over three experiments ± 2 %. [c] Collective yield of dehydration products 2,5-anhydroxylose and furfural. [d] Selectivity to furfural. [e] Furfural productivity calculated at the yield indicated and per gram of catalyst. [f] Furfural space-time-yield calculated for the yield indicated and monolithic reactor volume.

upon change of the reaction temperature, indicating that NbTiO-MNL2 was significantly the most efficient among the three monolithic catalysts. It turns out that, under identical flow conditions, use of NbTiO-MNL2 resulted in a much higher dehydration yield and furfural productivity. For the sake of comparison, selected data are shown in Table 6 for xylose conversions below 100%, wherein space-time-yields (STY, $kg_{furfural}$ $L_{reactor}^{-1}$ h^{-1}) and furfural productivities are reported. Test reactions in batch conditions confirmed this trend. The above results indicate that the addition of as low as 2% wt niobia into the titania lattice had a dramatic effect on the catalytic performance of the monoliths. A possible explanation can be found in the different acidic properties of the materials. Inspection of data reveals that the productivity of furfural is closely related to the LAS/BAS ratio in the monolithic catalysts. STY results are shown in Figure 11 as illustrative example. The higher the ratio, the higher was the reactor productivity. By contrast, no direct connection was highlighted between productivity and total number of acidic sites. These findings confirm that the dehydration reaction of xylose over heterogeneous catalysts is ruled by subtle combinations of their acidic properties.[147] Similar conclusions were previously reported using batch setups, wherein higher LAS/BAS ratios resulted in higher catalytic activity and in a lower selectivity, respectively, however using inhomogeneous acid series (i.e. Zr or Nb phosphate, sulfated zirconia, SiO_2-Al_2O_3, WO_x/ZrO_2, γ-Al_2O_3, HY or Hβ zeolites).[148]

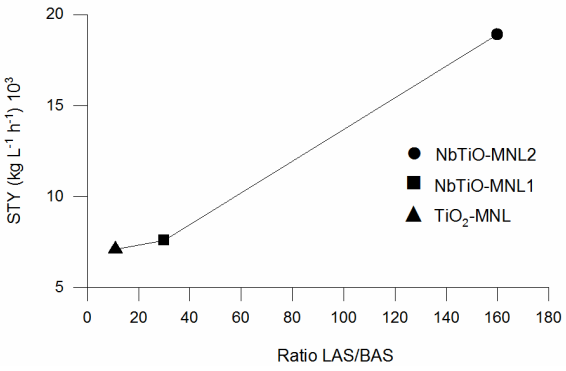

Figure 11. Relationship between LAS / BAS ratio and space-time-yield for the continuous flow dehydration reaction of xylose to furfural using monolithic catalysts under the same flow conditions (τ = 106 s, 130 °C). Data from Table 5 and 6.

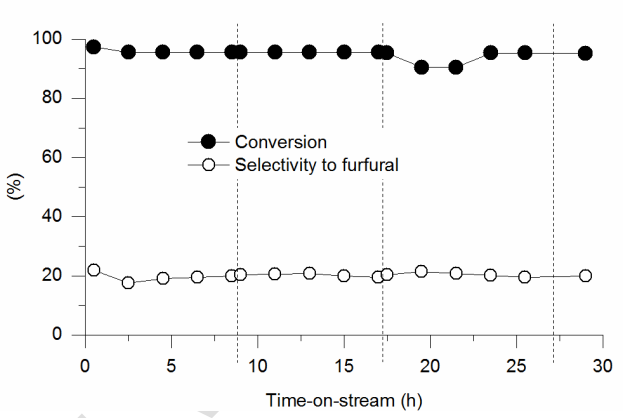

Figure 12. Continuous flow catalytic dehydration reaction of xylose over NbTiO-MNL2 monolith (τ 72 s, 130 °C, xylose 0.02 M in H_2O : GVL = 1:9 v/v, 0.3 mL min^{-1}, 276 mg catalyst). Effect of time-on-stream. Drop lines represent overnight switch-offs.

Catalyst resistance. The monolithic catalysts were typically tested for 8 hours continuous flow reaction time. Negligible catalytic activity and selectivity decreases were observed up to 4 days usage. Selected data are reported in Figure 12 for NbTiO-MNL2 catalyst under 130 °C and 72 s residence time, as representative example. The system was switched off overnight (due to safety reasons) and restart the day after under the same conditions. After four days and 29 hours overall time-on-stream, conversion and selectivity observed were 95 ± 2% and 20 ± 1 %, respectively, with > 98 % retention of the starting catalytic efficiency. In no circumstance niobium or titanium above the detection limit of ICP-OES were detected in the reaction solution recovered. These results indicate the stability of the monolithic catalysts under the reaction conditions adopted, as well as their resistance to pore blocking by coke and humins, as usually observed in the dehydration reaction of carbohydrates.[149] Despite no catalyst regeneration was required within the above reaction time span, the starting white colour of the catalysts could be restored by calcination at 350 °C for 2 hours, that indicates the possibility to remove the adsorbed humins.

Several heterogeneous catalysts have been reported for the dehydration reaction of xylose to furfural under batch conditions, including conventional TiO_2,[150] Nb_2O_5,[151] solid-supported Nb_2O_5 powders (silica, alumina, zirconia)[152,153,154] and titanoniobate nanosheets.[155] A detailed discussion of these catalysts is outside the scope

of the present manuscript and comprehensive reviews can be found in recent papers.[116,131,156,157] Nonetheless, it must be noticed that the large majority of these systems use biphasic solvent conditions (e.g. water-toluene / methyl isobutyl ketone / butanol) or harmful organic solvents (DMF, DMSO). Monophasic aqueous systems (e.g. water, water-GVL) require mild (110-150 °C) to harsh conditions (170-250 °C) to achieve poor (10-14 %) and moderate to good (29-62%) yields of furfural, respectively. Best results were obtained using zeolite beta nanocrystals (77% @ 170 °C, water)[158] or H-mordenite (81% @ 175 °C, 10% wt H_2O in GVL) catalysts.[159]

To the best of our knowledge, only one continuous flow system has been previously reported, based on modified tantalum oxide, for the catalytic conversion of xylose to furfural.[160] The conversion and selectivity trends with reaction temperatures and residence times were similar to those herein described. An optimized furfural yield of 59% at 96% xylose conversion was obtained under 180 °C and 3600 s residence time, using a H_2O-butanol 1:1.5 (v/v) biphasic solvent mixture and 20 bar N_2 backpressure. No details of the by-products observed were given.

The monolithic reactor herein described compares favourably with the performances reported for batch catalysts in the low temperature range, with the benefits of continuous flow operations, use of monophasic, safe reaction solvent and short reaction times.

Conclusions

The design of sustainable processes for the conversion of biomass to useful chemicals has been identified as a priority in the biorefinery industry.[111,161] To this aim, the development of heterogeneous acid catalysts featuring high resistance to water and efficiency under mild reaction conditions is deemed critical.

We have reported the synthesis and characterization of unconventional, mixed niobia-titania monolithic catalysts and their application to the dehydration reaction of xylose to furfural under continuous flow conditions. Materials with up to 2% wt niobium content feature a well-defined and isotropic, hierarchically porous network of interconnected mesopores and macropores. The results indicate that, at this Nb loading, Ti^{4+} ions are substituted by Nb^{5+} ions in the TiO_2 anatase lattice. The Lewis / Brønsted acid sites ratio shows to increase with increasing Nb content. The textural properties of the monoliths, while granting effective interaction between reactants and active sites, allow to minimize mass transfer limitations and pore blocking typical of mesoporous materials, thus resulting in no significant back pressure evolution under a continuous flow of a fluidic phase.

The catalytic dehydration reaction of xylose to furfural was conveniently achieved under mild reaction conditions, using H_2O:GVL as safe, single mobile phase, wherein adoption of continuous flow arrangement represents a significant process intensification. Addition of as low as 2% wt niobia to the titania lattice showed to dramatically improve the efficiency of the catalyst. Use of a homogenous series of materials sharing the same textural properties, allowed to identify the LAS/BAS ratio as the critical parameter in determining the catalytic performance. A non-optimized furfural yield of 39% under 140 °C reaction temperature and 224 s residence time was obtained using the catalyst with the higher LAS/BAS ratio without separation / purification steps.

Unprecedented interception of the 2,5-anhydroxylose intermediate suggests the reaction to occur via a cyclic dehydration mechanism with a significant contribution of xylose-xylulose isomerisation. No catalyst deactivation was observed over four days usage, demonstrating a remarkable stability of the catalyst in the aqueous phase and its resistance to poisoning by side products.

The performance of the catalyst herein described compares favourably with that of the heterogeneous systems reported in the literature, whereas the dehydration reaction is usually carried out in batch using biphasic / toxic solvents (toluene, DMF, butanol), higher temperatures, or in the homogenous phase using mineral acids.

These results may help in the design and in the development of more sustainable catalytic processes for the production of useful platform chemicals and fuels from renewable biomass.

Experimental

General information

Hierarchical meso / macroporous titania monoliths (TiO_2-MNL) were prepared as previously described.[46] Details of experimental methods are reported in the Supporting Information.

Synthesis of hierarchically porous niobia-titania monoliths

Meso-/macroporous mixed niobia-titania monoliths (NbTiO-MNL) were prepared as follows. All the reagents were cooled down to 0 °C prior of use and maintained at that temperature using an ice bath during the whole procedure. In a typical synthesis, two separate solutions were prepared: A) a selected amount of $NbCl_5$ was dissolved in 1.14 g of 37% HCl (11.6 mmol); B) 0.38g of polyethylene oxide (PEO, 0.039 mmol) were dissolved in 1.72 g of distilled water (135.5 mmol). The solutions A and B were added in the order at 0 °C to $Ti(OPr)_4$ (TPO, 6.96 g, 24.0 mmol) under vigorous stirring. The mixture was stirred for 2-3 minutes. N-Methylformamide (NMFA, 1.09 g, 18.3 mmol) was added dropwise with stirring until a clear solution was obtained. The molar ratio composition of the mixture was: 1 Ti / x Nb /0.48 HCl / 5.64 H_2O / 0.76 NMFA / 0.0016 PEO, with x = 0.0 - 0.01 - 0.02. The mixture was then poured into a polypropylene tube (inner diameter 6-7 mm, length 4 cm), which was sealed and kept at 40 ºC during 24 h for gelation and phase separation. The resulting gel was aged at 60 ºC for 24 h (heating ramp = 1°C/min). The wet monolith obtained was removed from the mould and washed with 1-propanol (5 x 25 mL, room temperature), before being dried at room temperature for 24 h and at 40 ºC for 1 week. The final white monolith was obtained after calcination of the solid at 350 ºC for 5 h (heating ramp = 0.5 ºC/min).

Catalytic reactions in continuous flow mode

Catalytic reactions under continuous flow conditions were carried out in air atmosphere using a home-made, metal-free continuous-flow reactor system (Scheme S1). The reaction temperature was regulated using an oven comprising a Kapton® flexible heating element and a temperature controller accurate ± 0.1 °C. In a typical experiment, a sample of monolithic catalyst (5 mm diameter, 7 mm length, 114 mg, volume 137 μL), was cladded with a heat-shrinkable PTFE tube and connected to the continuous flow system via 1/16" PEEK tubing. A solution of xylose in H_2O : GVL = 1 : 9 (v/v) was allowed to flow through the monolith. Residence times were in the range 70 - 224 s, corresponding to 0.1 - 0.4 mL min^{-1} substrate solution flow rate. The attainment of steady state conditions (ca. 0.5 h) was taken as the reaction start time. At the outlet of the reactor, the reaction solution was cooled down to room temperature and periodically analyzed for conversion and selectivity by GC, GC-MS and HPLC. Aliquots were sampled at 1 h intervals for Nb and Ti leaching determination by ICP-OES. The reaction products were unequivocally identified by comparison of the GC and HPLC retention times and mass spectra with those of authentic specimens. Quantitative analyses were carried out via HPLC and GC based on calibration curves of the pure compounds.

Acknowledgements

Thanks are due to: Dr. Samuele Ciattini (Centro di Cristallografia University of Firenze, Italy) for X-ray tomography measurements, Centro Microscopie Elettroniche (CNR, Firenze, Italy) for technical assistance, Dr. Andreana Piancastelli (ISTEC - CNR, Faenza, Italy) for Hg intrusion measurements, Dr. A. Ienco (ICCOM-CNR) for XRD discussion, C. Almansa (SSTTI Universidad de Alicante) for TEM analysis. F.B. thank financial support from EIT Raw Materials through project FREECATS (Project no. 15054).

Conflicts of interest

The authors declare no conflict of interest.

Keywords: sustainable chemistry • heterogeneous catalysis • biorenewable resources • continuous flow • xylose

Abbreviations: HPLC, high-performance liquid chromatography, ICP-OES, Inductively Coupled Plasma Atomic Emission Spectroscopy; BET, Brunauer–Emmett–Teller model; ESEM, Environmental Scanning Electron Microscopy; EDS, Energy Dispersive X-ray Spectrometry; TEM, Transmission Electron Microscopy; XRD, X-ray diffraction; XPS, X-ray Photoelectron spectroscopy; GVL, γ-valerolactone; GC, gas chromatography; GC-MS, gas chromatography-mass spectrometry; STY, space-time-yield.

[1] R. J. Jones, Definitions of Terms Relating to the Structural and Processing of Sols, Gels, Networks and Inorganic–Organic Hybrid Materials. IUPAC Recommendations. *Pure Appl. Chem*. **2007**, *79*, 1801-1829.
[2] A. Cybulski, J. A. Moulijn, *Structured Catalysts and Reactors,* Marcel Dekker Ltd.: New York, 2005, p 19.
[3] R. M. Heck, S. Gulati, R. J.Farrauto, *Chem. Eng. J.* **2001**, *82*, 149-156.
[4] T. Vesna, J. Franjo, *Appl. Catal., A* **2006**, *311*, 112-121.
[5] K. Nakanishi, in *Hierarchically Structured Porous Materials*, B. Su, C. Sanchez, X., Yang, Eds.; Wiley-VCH, Weinheim, 2012, Chapter 8.
[6] C. M. A. Parlett, K.Wilson A. F. Lee, *Chem. Soc. Rev.* **2013**, *42*, 3876-3893.
[7] A. Feinle, M. S. Elsaesser, N. Hüsing, *Chem. Soc. Rev*. **2016**, *45*, 3377-3399.
[8] A. Galarneau, A. Sachse, B. Said, C. H. Pelisson, P. Boscaro, N. Brun, L. Courtheoux, N. Olivi-Tran, B. Coasne, F. Fajula, *C. R. Chimie* **2016**, *19*, 231-247.
[9] A. Galarneau, Z. Abid, B. Said, Y. Didi, K. Szymanska, A. Jarzebski, F. Tancret, H. Hamaizi, A. Bengueddach, F. Di Renzo, F. Fajula *Inorganics* **2016**, *4*, 9-34.
[10] M. Guisnet, M. Guidotti, *Microporous and Mesoporous Solid Catalysts*, in *Catalysts for Fine Chemical Synthesis*, Vol. 4, E. G. Derouane, Ed.; John Wiley & Sons, Weinheim, 2006, Chapter 2.
[11] B. Louis, G. Laugel, P. Pale, M. Maciel Pereira *ChemCatChem* **2011**, *3*, 1263-1272
[12] H. Minakuchi, K. Nakanishi, N. Soga, N. Ishizuka, N.Tanaka, *J. Chromatogr. A* **1997**, *762*, 135-146.
[13] S. Whitaker, *Transport Porous Med.* **1986**, *1*, 3-25.
[14] C. Wiles, P. Watts, *Green Chem.* **2014**, *16*, 55-62.
[15] R. M. Myers, D. E. Fitzpatrick, R. M. Turner, S. V. Ley, *Chem. Eur. J.* **2014**, *20*, 12348-12366.
[16] N. G. Anderson, *Org. Process Res. Dev*. **2012**, *16*, 852-869.
[17] A. Stankiewicz, *Chem. Eng. Sci.* **2001**, *56*, 359-364.
[18] M. R. Buchmeiser, *Polymer* **2007**, *48*, 2187-2198.
[19] M. Baumann, I. R. Baxendale, S. V. Ley, N. Nikbin, C.D. Smith, *Org. Biomol. Chem*. **2008**, *6*, 1587-1593.
[20] F. Svec, T.B. Tennikova, Z. Deyl, *Monolithic Materials: Preparation, Properties, and Applications,* Elsevier, Amsterdam, 2003.
[21] S. Xie, R.W. Allington, J.M. Fréchet, F. Svec in *Advances in Biochemical Engineering/Biotechnology,* R. Freitag, Ed., Springer, London, 2002.
[22] K. Nakanishi, H. Shikata, N. Ishizuka, N. Koheiya, N. Soga, *J. High Resol. Chromatogr*. **2000**, *23*, 106-110.
[23] B. Gaweł, K.Gaweł, G. Øye, *Materials* **2010**, *3*, 2815-2833.
[24] J. Babin, J. Iapichella, B. Lefèvre, C. Biolley, J. P. Bellat, F. Fajula, A. Galarneau, *New J. Chem*. **2007**, **31**, 1907-1917.
[25] T. Amatani, K. Nakanishi, K. Hirao, T. Kodaira, *Chem. Mater.* **2005**, *17,* 2114-2119.
[26] X. Guo, R. Wang, H. Yu, Y. Zhu, K. Nakanishi, K. Kanamori, H. Yang, *Dalton Trans*. **2015**, *44*, 13592-13601.
[27] S. Hartmann, M. S. Elsaesser, N. Hüsing, *Z. Anorg. Allg. Chem.* **2014**, *640*, 641-648.
[28] S. Hartmann, A. Sachse, A. Galarneau, *Materials* **2012**, *5*, 336-349.
[29] B. Gaweł, G. Øye, *Mater. Lett*. **2013**, *95*, 86-88.
[30] B. Gaweł, K. Gaweł, T. C. Hobæk, M. Yasuda, G. Øye, *Mater. Chem. Phys.* **2012**, *137*, 414-420.
[31] G. Hasegawa, K. Kanamori, K. Nakanishi, T. Hanada, *J. Am. Ceram. Soc.* **2010**, *93* 3110-3115.
[32] J. Konishi, K. Fujita, K.Nakanishi, K. Hirao, *Chem. Mater.* **2006**, *18*, 6069-6074.
[33] Y. Zhu, T. Shimizu, T. Kitajima, K. Morisato, N.Moitra, N.Brun, T. Kiyomura, K. Kanamori, K. Takeda, H. Kurata, M.Tafu, K. Nakanishi, *New J. Chem*. **2015**, *39*, 2444-2450.
[34] X. Cai, W. Zhu, H. Yang, C. Xu, K. Nakanishi, K. Kanamori, X. Guo, *New J. Chem*. **2015**, *39*, 6238-6243.
[35] Organic-inorganic silsesquioxane hybrids have also been described, see: N. Moitra, K. Kanamori, T. Shimada, K. Takeda, Y. H. Ikuhara, X. Gao, K. Nakanishi, *Adv. Funct. Mater.* **2013**, *23*, 2714-2722.
[36] MOF-based monolith have been reported, see: N. Moitra, S. Fukumoto, J. Reboul, K. Sumida, Y. Zhu, K. Nakanishi, S. Furukawa, S. Kitagawa, K. Kanamori, *Chem. Commun*. **2015**, *51*, 3511-3514.
[37] J. Wegner, S. Ceylan, A. Kirschning, *Chem. Commun*. **2011**, *47*, 4583-4592.
[38] R. Ricciardi, J. Huskens, W. Verboom, *ChemSusChem* **2015**, *8*, 2586-2605.
[39] K. Nakanishi, *J. Porous Mat.* **1997**, *4*, 67-112.

[40] A. Sachse, A. Galarneau, B. Coq, F. Fajula, *New J. Chem*. **2011**, *35*, 259-264.

[41] H. Yu, Y. Zhu, H. Yang, K. Nakanishi, K. Kanamori, X. Guo, *Dalton Trans*. **2014**, *43*, 12648-12656.

[42] P. He, S. J. Haswell, P. D. I. Fletcher, S. M. Kelly, A. Mansfield, *Beilstein J. Org. Chem.* **2011**, *7*, 1150-1157.

[43] C. H. Pélisson, T. Nakanishi, Y. Zhu, K. Morisato, T. Kamei, A. Maeno, H. Kaji, S. Muroyama, M. Tafu, K. Kanamori, T. Shimada, K. Nakanishi, *ACS Appl. Mater. Interfaces* **2017**, *9*, 406-412.

[44] A. Sachse, V. Hulea, A. Finiels, B. Coq, F. Fajula, A. Galarneau *J. Catal.* **2012**, *287*, 62-67.

[45] Y. Zhu, K. Kanamori, N. Brun, C. H. Pélisson, N. Moitra, F. Fajula, V. Hulea, A. Galarneau, K. Takeda, K. Nakanishi, *Catal. Commun.* **2016**, *87*, 112-115

[46] N. Linares, S. Hartmann, A. Galarneau, P. Barbaro, *ACS Catal.* **2012**, *2*, 2194-2198.

[47] A. Sachse, N. Linares, P. Barbaro, F. Fajula, A. Galarneau, *Dalton Trans.* **2013**, *42*, 1378-1384.

[48] A. El Kadib, R. Chimenton, A. Sachse, F. Fajula, A.Galarneau, B. Coq *Angew. Chem. Int. Ed*. **2009**, *48*, 4969-4972.

[49] C. P. Haas, T. Müllner, R. Kohns, D. Enkeb, U. Tallarek, *React. Chem. Eng*. **2017**, *2*, 498-511.

[50] A. Sachse, A. Galarneau, F. Fajula, F. Di Renzo, P. Creux, B. Coq, *Micropor. Mesopor. Mater.* **2011**, *140*, 58-68.

[51] A. Sachse, R. Ameloot, B. Coq, F. Fajula, B. Coasne, D. De Vos, A. Galarneau, *Chem. Commun.* **2012**, *48*, 4749-4751.

[52] F. Liguori, P. Barbaro, B. Said, A. Galarneau, V. Dal Santo, E. Passaglia, A. Feis, *ChemCatChem* **2017**, *9*, 3245-3258.

[53] A. J. Grano, F. M. Sayler, J. H. Smått, M. G.Bakker, *J. Porous Mater.* **2014**, *21*, 1113-1122.

[54] A. Corma, *Chem. Rev*. **1995**, *95*, 559-614.

[55] G. Busca, *Chem. Rev.* **2007**, *107*, 5366-5410.

[56] P. Gupta, S. Paul, *Catal. Today* **2014**, *236*, 153-170.

[57] K. Shimizu, A. Satsuma, *Energy Environ. Sci.* **2011**, *4*, 3140-3153.

[58] R. A. Sheldon, *Green Chem.* **2014**, *16*, 950-963.

[59] A. Koreniuk, K. Maresz, K. Odrozek, A. B. Jarzębski, J.Mrowiec-Białoń, *Appl. Catal. A: Gen.* **2015**, *489*, 203-208.

[60] X. Chen, S. S. Mao, *Chem. Rev.* **2007**, *107*, 2891-2959.

[61] U. Diebold, *Surf. Sci. Rep.* **2003**, *48*, 53-229.

[62] K. Tanabe, *Catal. Today* **2003**, *78*, 65-77.

[63] I. Nowak, M. Ziolek, *Chem. Rev*. **1999**, *99*, 3603-3624.

[64] T. Okuhara, *Chem. Rev*. **2002**, *102*, 3641-3666.

[65] M. Ziolek, *Catal. Today* **2003**, *78*, 47-64.

[66] Y. Zhao, X. Zhou, L. Ye, S. C. E. Tsang, *Nano Reviews* **2012**, *3*, 17631.

[67] P. Carniti, A. Gervasini, S. Biella, A. Auroux, *Catal. Today* **2006**, *118*, 373-378.

[68] A. Lewera, L. Timperman, A. Roguska, N. Alonso-Vante, *J. Phys. Chem. C* **2011**, *115*, 20153-20159

[69] E. I. Ko, R. Bafrali, N. T. Nuhfer, N. J. Wagner, *J. Catal.* **1985**, *95*, 260-270.

[70] T. Beutel, V. Siborov, B. Tesche, H. Knözinger, *J. Catal.* **1997**, *167*, 379-390.

[71] T. Hoffer, S. Dobos, L. Guczi, *Catal. Today* **1993**, *16*, 435-446.

[72] *Materials for Energy Conversion Devices*, C. C. Sorrell, J. Nowotny, S. Sugihara, Eds., CRC Press, Boca Raton, 2005.

[73] A. L. Linsebigler, G. Lu, J. T. Jr. Yates, *Chem. Rev*. **1995**, *95*, 735-758.

[74] R. M. Pittman, A. T. Bell, *Catal. Lett.* **1994**, *24*, 1-13.

[75] M. Franco Finol, J. Rooke, B. L. Su, M. Trentesaux, J. M. Giraudon, J. F. Lamonier, *Catal. Today* **2012**, *192*, 154-159.

[76] Niobium-doped titanates have also been described, see e.g.: E. Wada, M. Kitano, K. Yamamoto, K. Nakajima, S. Hayashi, M. Hara, *Catal. Sci. Technol.* **2016**, *6*, 4832–4839.

[77] M.Z. Atashbar, H.T. Sun, B. Gong, W. Wlodarski, R. Lamb *Thin Solid Films* **1998**, *326*, 238-244.

[78] A. Mattsson, M. Leideborg, K. Larsson, G. Westin, L. Österlund, *J. Phys. Chem. B* **2006**, *110*, 1210-1220.

[79] D. Morris, Y. Dou, J. Rebane, C.E.J. Mitchell, R.G. Egdell, D.S.L. Law, A. Vitadini, M. Casarin, *Phys. Rev. B* **2000**, *61*, 13445-13457.

[80] Y. Wang, B.M. Smarsly, I. Djerdj, *Chem. Mater*. **2010**, *22*, 6624-6631.

[81] W. Zeng, T. Liu, Z. Wang, *Sensor. Actuat. B: Chem*. **2012**, *166-167*, 141-149.

[82] S. Hasegawa, H. Aritani, M. Kudo, *Catal. Today* **1993**, *16*, 371-377.

[83] A. Kubacka, G. Colón, M. Fernández-García *Catal. Today* **2009**, *143*, 286-292.

[84] P. Viparelli, P. Ciambelli, J. C. Volta, J. M. Herrmann, *Appl. Catal. A: Gen.* **1999**, *182*, 165-173.

[85] M. Franco Finol, J. Rooke, S. Siffert, R. Cousin, P. Carniti, A. Gervasini, J. M. Giraudon, B. L. Su, J. F. Lamonier, *New J. Chem.* **2014**, *38*, 1988-1995.

[86] T. Onfroy, O. V. Manoilova, S. B. Bukallah, D. M. Hercules, G. Clet, M. Houalla, *Appl. Catal. A: Gen.* **2007**, *316*, 184-190.

[87] J. C. Rooke, T. Barakat, M. Franco Finol, P. Billemont, G. De Weireld, Y. Lie, R. Cousin, J. M. Giraudon, S. Siffert, J. F. Lamonier, B.L. Su *Appl. Catal. B: Environ*. **2013**, *142-143*, 149-160.

[88] J. Konishi, K. Fujita, K. Nakanishi, K. Hirao, K. Morisato, S. Miyazaki, M. Ohira, *J. Chromatogr. A* **2009**, *1216*, 7375-7383.

[89] K. Tanabe, *Catal. Today* **1990**, *8*, 1-11.

[90] T. Iizuka, K. Ogasawara, K. Tanabe, *Bull. Chem. Soc. Jpn*. **1983**, *56*, 2927-2931.

[91] Y. Zhu, Y. Morimoto, T. Shimizu, K. Morisato, K. Takeda, K. Kanamori, K. Nakanishi, *J. Ceram. Soc. Jpn*. **2015**, *123*, 770-778.

[92] Mixed niobia-titania monoliths with 5 and 10% wt Nb content were also synthesized and characterized. However, slight differences in the pH and phase system, due to the synthetic protocol, resulted skeletons made of globular aggregates. This led to brittle materials unsuitable for both cladding and continuous flow applications. Therefore, we decided not to investigate further NbTiO-MNL5 and NbTiO-MNL10 because of the poor mechanical stability. See also: J. Konishi, K. Fujita, K. Nakanishi, K. Hirao, *Chem. Mater.* **2006**, *18*, 864-866.

[93] Y. Liu, J. M. Szeifert, J. M. Feckl, B. Mandlmeier, J. Rathousky, O. Hayden, D. Fattakhova-Rohlfing, T. Bein, *ACS Nano* **2010**, *4*, 5373-5381.

[94] X. Lu, X. Mou, J. Wu, D. Zhang, L. Zhang, F. Huang, F. Xu, S. Huang, *Adv. Funct. Mater*. **2010**, *20*, 509-515.

[95] N. Özer, D. G. Chen, C. M. Lampert, *Thin Solid Films* **1996**, *277*, 162-168.

[96] G. M. Ingo, S. Dirè, F. Babonneau, *Appl. Surf. Sci.* **1993**, *70*, 230-234.

[97] L. Sheppard, T. Bak, J. Nowotny, C.C. Sorrell, S. Kumar, A. R. Gerson, M. C. Barnes, C. Ball, *Thin Solid Films* **2006**, *510*, 119-124.

[98] T. Bak, J. Nowotny, M. Rekas, C.C. Sorrell, *J. Phys. Chem. Solids* **2003**, *64*, 1057-1067.

[99] V. León, *Surf. Sci.* **1995**, *339*, L931–L934.

[100] M. Tamura, K. Shimizu, A. Satsuma, *Appl. Catal. A: Gen*. **2012**, *433*, 135-145.

[101] C. A. Emeis, *J. Catal.* **1993**, *141*, 347-354.

[102] A. Chareonlimkun, V. Champreda, A. Shotipruk, N. Laosiripojana, *Bioresour. Technol.* **2010**, *101*, 4179-4186.

[103] S. Dutta, S. De, A. K. Patra, M. Sasidharan, A. Bhaumik, B. Saha, *Appl. Catal. A* **2011**, *409-410*, 133-139.

[104] K. Nakajima, Y. Baba, R. Noma, M. Kitano, J. N. Kondo, S. Hayashi, M. Hara, *J. Am. Chem. Soc.* **2011**, *133*, 4224-4227.

[105] J. M. Jehng, I. E. Wachs, *J. Phys. Chem*. **1991**, *95*, 7373-7379.

[106] A. Gervasini, P. Carniti, M. Marzo, A. Auroux, *J. Catal*. **2012**, *296*, 143-155.

[107] K. Nakajima, J. Hirata, M. Kim, N. K. Gupta, T. Murayama, A. Yoshida, N. Hiyoshi, A. Fukuoka, W. Ueda, *ACS Catal.* **2018**, *8*, 283-290.

[108] J. Datka, A. M. Turek, J. M. Jehng, I.E. Wachs, *J. Catal.* **1992**, *135*, 186-199.

[109] R. Luque, *Curr. Opin. Green Sustain. Chem.* **2016**, *2*, 6-9.

[110] M. J. Climent, A. Corma, S. Iborra, *Green Chem.* **2014**, *16*, 516-547.

111] J. J. Bozell, G. R. Petersen, *Green Chem*. **2010**, *12*, 539-554.

[112] A.S. Mamman, J.M. Lee, Y.C. Kim, I.T. Hwang, N.J. Park, Y.K. Hwang, J.S. Chang, J. S. Hwang, *Biofuels Bioprod. Biorefin.* **2008**, *2*, 438-454.

[113] K J. Zeitsch, *The chemistry and technology of furfural and its many by-products.* Volume 13. Amsterdam, Elsevier, 2000.

[114] C. M. Cai, T. Zhang, R. Kumar, C. E. Wyman, *J. Chem. Technol. Biotechnol*. **2014**, *89*, 2-10.

[115] R. Mariscal, P. Maireles-Torres, M. Ojeda, I. Sádaba, M. López Granados *Energy Environ. Sci.* **2016**, *9*, 1144-1189.

[116] K. Yan, G. Wu, T. Lafleur, C. Jarvis, *Renew. Sust. Energ. Rev.* **2014**, *38*, 663-676.

[117] B. Danon, G. Marcotullio, W. de Jong *Green Chem*. **2014**, *16*, 39-54.

[118] K. R. Enslow, A. T. Bell, *ChemCatChem* **2015**, *7*, 479-489.

[119] M. B. Fusaro, V. Chagnault, D. Postel, *Carbohydr. Res.* **2015**, *409*, 9-19.

[120] V. Choudhary, S. I. Sandler, D. G. Vlachos, *ACS Catal*. **2012**, *2*, 2022-2028.

[121] M. S. Holm, Y. J. Pagán-Torres, S. Saravanamurugan, A. Riisager, J. A. Dumesic, E. Taarning, *Green Chem*. **2012**, *14*, 702-706.

[122] K. Lamminpää, J. Ahola, J. Tanskanen, *RSC Adv.* **2014**, *4*, 60243-60248.

[123] L. Filiciotto, A. M. Balu, J. C. Van der Waal, R. Luque, *Catal. Today* **2018**, *302*, 2-15.

[124] S. M. Walas, *Chemical Process Equipment. Selection and Design.* Butterworth-Heinemann, Washington, 1990, Chapter 17.

[125] J. N. Chheda, Y. Román-Leshkov, J. A. Dumesic, *Green Chem*. **2007**, *9*, 342-350.

[126] A.S. Dias, M. Pillinger, A. A. Valente, *Appl. Catal. A: Gen.* **2005**, *285*, 126-131.

[127] F. Liguori, C. Moreno-Marrodan, P. Barbaro, *ACS Catal*. **2015**, *5*, 1882-1894.

[128] I. T. Horváth, H. Mehdi, V. Fabos, L. Boda, L. T. Mika, *Green Chem.* **2008**, *10*, 238-242.

[129] M. A. Mellmer, C. Sener, J. M. R. Gallo, J. S. Luterbacher, D. M. Alonso, J. A. Dumesic, *Angew. Chem. Int. Ed.* **2014**, *53*, 11872-11875.

[130] X. Hu, C. Lievens, C. Z. Li, *ChemSusChem* **2012**, *5*, 1427-1434.

[131] X. Zhang, K. Wilson, A. F. Lee, *Chem. Rev*. **2016**, *116*, 12328-12368.

[132] A.S. Dias, S. Lima, M. Pillinger, A. A. Valente, in *Ideas in Chemistry and MolecularSciences: Advances in Synthetic Chemistry*, B. Pignataro, Ed., Wiley-VCH, Weinheim, 2010, Chapter 8.

[133] K. Dussan, B. Girisuta, M. Lopes, J. J. Leahy, M. H. B. Hayes, *ChemSusChem* **2015**, *8*, 1411-1428.

[134] W. Zhang, Y. Zhu, S. Niu, Y. Li, *J. Mol. Cat. A: Chemical* **2011**, *335*, 71-81.

[135] M. J. Jr. Antal, T. Leesomboon, W. S. Mok, G. N. Richards, *Carbohyd. Res.* **1991**, *217*, 71-85.

[136] P. Barbaro, F. Liguori, C. Moreno-Marrodan, *Green Chem*. **2016**, *18*, 2935-2940.

[137] J. U. Oltmanns, S. Palkovits, R. Palkovits, *Appl. Catal. A: Gen.* **2013**, *456*, 168-173.

[138] S. Verma, R. B. N. Baig, M. N. Nadagouda, C. Len, R. S. Varma, *Green Chem*. **2017**, *19*, 164-168.

[139] L. Hu, G. Zhao, W. Hao, X. Tang, Y. Sun, L. Lin, S. Liu, *RSC Adv.* **2012**, *2*, 11184-11206.

[140] M. R. Nimlos, X. Qian, M. Davis, M. E. Himmel, D. K. Johnson, *J. Phys. Chem. A* **2006**, *110*, 11824-11838.

[141] T. Ahmad, L. Kenne, K. Olsson, O. Theander, *Carbohydr. Res*. **1995**, *276*, 309-320.

[142] Y. Yang, C. W. Hu, M. M. Abu-Omar, *ChemSusChem* **2012**, *5*, 405-410.

[143] V. Choudhary, A. B. Pinar, S. I. Sandler, D. G. Vlachos, R. F. Lobo, *ACS Catal*. **2011**, *1*, 1724-1728.

[144] O. Ershova, J. Kanervo, S. Hellstena, H. Sixta, *RSC Adv*. **2015**, *5*, 66727-66737.

[145] K. Stensrud, (Archer Daniels Midland Company). Patent No. WO2017/30684 A1, 2017.

[146] M. H. L. Silveira, B. A. Vanelli, M. L. Corazza, L. Pereira Ramos, *Bioresource Technol.* **2015**, *192*, 389-396.

[147] R. Weingarten, G. A. Tompsett, W. C. Jr. Conner, G. W Huber, *J. Catal.* **2011**, *279*, 174-182.

[148] B. Pholjaroen, N. Li, Z. Wang, A. Wang, T. Zhang, *J. Energy Chem.* **2013**, *22*, 826-832.

[149] S. Lima, M. Pillinger, A. A. Valente, *Catal. Commun.* **2008**, *9*, 2144-2148.

[150] N. K. Gupta, A. Fukuoka, K. Nakajima, *ACS Catal.* **2017**, *7*, 2430-2436.

[151] C. García-Sancho, J. M. Rubio-Caballero, J. M. Mérida-Robles, R. Moreno-Tost, J. Santamaría-González, P. Maireles-Torres, *Catal. Today* **2014**, *234*, 119-124.

[152] M. J. Campos Molina, M. López Granados, A. Gervasini, P. Carniti, *Catal. Today* **2015**, *254*, 90-98.

[153] C. García-Sancho, I. Agirrezabal-Telleria, M. B. Güemez, P. Maireles-Torres, *Appl. Catal. B: Environ*. **2014**, *152-153*, 1-10

[154] I. Agirrezabal-Telleria, C. García-Sancho, P. Maireles-Torres, P. L. Arias, *Chinese J. Catal.* **2013**, *34*, 1402-1406.

[155] A.S. Dias, S. Lima, D. Carriazo, V. Rives, M. Pillinger, A. A. Valente, *J. Catal.* **2006**, *244*, 230-237.

[156] X. Li, P. Jia, T. Wang, *ACS Catal.* **2016**, *6*, 7621-7640.

[157] I. Agirrezabal-Telleria, I. Gandarias, P.L. Arias, *Catal. Today* **2014**, *234*, 42-58.

[158] L. R. Ferreira, S. Lima, P. Neves, M. M. Antunes, S. M. Rocha, M. Pillinger, I. Portugal, A. A. Valente, *Chem. Eng. J.* **2013**, *215-216*, 772-783.

[159] E. I. Gürbüz, J. M. R. Gallo, D. M. Alonso, S. G. Wettstein, W. Y. Lim, J. A. Dumesic, *Angew. Chem. Int. Ed.* **2013**, *52*, 1270-1274.

[160] X. Li, L. T. Pan, J. Deng, Y. Fu, H. J. Xu, *RSC Adv.* **2015**, *5*, 70139-70146.

[161] *A Roadmap for moving to a competitive low carbon economy in 2050*, European Commission, COM(2011) 112 final.